Available online at www.sciencedirect.com
ScienceDirect
Proceedings of the Combustion Institute 000 (2016) 1–9
Proceedings of the Combustion Institute
www.elsevier.com/locate/proci

Effects of flame propagation speed and chamber size on end-gas autoignition

Hao Yu, Chengken Qi, Zheng Chen*

SKLTCS, Department of Mechanics and Engineering Science, College of Engineering, Peking University, Beijing 100871, China

Received 29 November 2015; accepted 28 July 2016
Available online xxx

Abstract

End-gas autoignition has direct relevance to engine knock and thereby has been extensively studied. However, in the literature there are still some contradictions on how different factors affect end-gas autoignition and knock intensity. Specifically, there is contradictory literature on (1) whether faster combustion may promote or inhibit end-gas autoignition and engine knock, and (2) whether knock intensity increases or decreases with burned mass fraction (BMF). To answer these two questions, one-dimensional flame propagation and end-gas autoignition in a closed cylindrical chamber are investigated and the effects of flame propagation speed and chamber size on end-gas autoignition are examined in this study. In the transient numerical simulation, two fuels, hydrogen and iso-octane, are studied; and detailed chemistry is considered. It is shown that if the flame propagation is fast enough or the chamber is small enough, end-gas autoignition and knock can be prevented; otherwise, the knock intensity may increase as the flame propagation speed increases or as the chamber size decreases. The maximum pressure is found to change non-monotonically with the BMF as well as the flame propagation speed and chamber size. This helps to explain why there is contradictory literature on those two questions mentioned above. The answers to these two questions depend on the amount of unburned mixture at the moment of end-gas autoignition: if there is enough unburned mixture before end-gas autoignition, the maximum pressure increases with the flame propagation speed and BMF; otherwise, the opposite trend occurs. Besides, comparison between the results for hydrogen and iso-octane indicates that end-gas chemical reaction and heat release occurring before autoignition can greatly reduce the maximum pressure.

Keywords: Autoignition; End-gas; Flame propagation speed; Chamber size; Maximum pressure

1. Introduction

When a premixed flame propagates in a closed chamber, the unburned gas (end-gas) is progressively compressed and its temperature and pressure continuously increase. Under certain conditions, the ignition delay time of end-gas might be shorter

* Corresponding author.
E-mail addresses: cz@pku.edu.cn, chenzheng@coe.pku.edu.cn (Z. Chen).

http://dx.doi.org/10.1016/j.proci.2016.07.123
1540-7489 © 2016 by The Combustion Institute. Published by Elsevier Inc.

than the time taken by the propagating flame to consume all the unburned mixture, and thereby autoignition might occur in end-gas.

End-gas autoignition has direct relevance to knock in spark ignition engines (SIE) [1–3]. Therefore, there are many studies on end-gas autoignition in the literature. Previous theoretical (e.g., [4–6]), experimental (e.g., [7, 8]) and numerical (e.g., [9–11]) works on end-gas autoignition were described in our recent paper [12] and thereby is not repeated here. Besides, direct numerical simulations (DNS) were conducted to study the combustion in Homogeneous Charge Compression-Ignition (HCCI), Spark-Assisted HCCI (SACI), and Reactivity Controlled Compression Ignition (RCCI) conditions. For examples, Bhagatwala et al. [26] conducted DNS of an autoignitive ethanol/air mixture in HCCI and SACI modes. In their simulation, source terms were included to emulate the compression and expansion due to piston motion. They demonstrated that compression heating has great impact on hear release profile. Bhagatwala et al. [27] conducted 1D and 2D DNS under RCCI conditions of a primary reference fuel (PRF) mixture. They observed both deflagration and spontaneous ignition fronts and analyzed the influence of n-heptane concentration, fuel-concentration stratification and pressure on the combustion modes. Yoo and coworkers [28, 29] examined the influence of temperature inhomogeneities and turbulence on the ignition in PRF HCCI combustion. They found that the influence of fuel composition on the ignition characteristics of PRF/air decreases greatly with thermal stratification. These studies are related to end-gas autoignition since both deflagration and autoignition modes are included.

Despite the extensive attention devoted to understanding end-gas autoignition and engine knock, there are still some disagreements or even contradictions on how different factors affect end-gas autoignition and knock intensity. For example, Chen and Raine [13] found that there is contradictory literature about whether faster combustion may promote or inhibit end-gas autoignition and engine knock. On one hand, faster flame propagation results in less time for end-gas autoignition and thereby knock may be suppressed (e.g., [14]). On the other hand, increasing the flame propagation speed makes the end-gas pressure and temperature rise more rapidly and thereby reduces the ignition delay time, which is favorable for end-gas autoignition and knock (e.g., [15]). Therefore, there is a need to investigate how flame propagation speed affect end-gas autoignition and knock intensity.

Besides, the knock intensity is considered to be strongly correlated with the amount of unburned or burned mixture at the moment of end-gas autoignition. Burned Mass Fraction (BMF, the mass fraction of burned gas at the moment of end-gas autoignition) is often used as an indicator for knock severity. However, there is contradictory literature on whether knock intensity increases or decreases with BMF. For examples, Robert et al. [16] demonstrated that the knock intensity increases as BMF decreases; while Kagan et al. [4] and Kagan and Sivashinsky [5] showed that knock intensity increases when BMF increases. It is therefore of interest to investigate how knock intensity changes with BMF.

The above-mentioned two contradictions constitute the motivation of the present work. The objective of this study is to clarify these contradictions. One-dimensional (1D) flame propagation and end-gas autoignition in a closed cylindrical chamber were investigated here. It is noted that autoignition in practical engines is a highly nonhomogeneous phenomenon. Since, turbulence variable chamber volume, boundary layer and wall heat transfer are not considered in the 1D model, engine combustion and knock cannot be fully represented by the present 1D model (therefore, 'maximum pressure' instead of 'knock intensity' is used for present simulation results). Nevertheless, such simple 1D model still helps to clarify the contradictions mentioned above since different effects can be isolated and quantified individually.

Besides the flame propagation speed, we also considered the chamber size since it also affects end-gas autoignition and BMF. Both theoretical analysis and numerical simulations were conducted to examine the effects of flame propagation speed and chamber size on end-gas autoignition and to elucidate the relationship between maximum pressure and BMF.

2. Theoretical analysis

We analyzed 1D laminar flame propagation and end-gas autoignition in a closed chamber: only 1D cylindrical geometry was considered here and similar analysis can be easily extended to planar and spherical geometries. It is noted that similar analysis was conducted before for laminar flame speed measurement using propagating spherical flames in a closed spherical chamber [17, 18] (but not for end-gas autoignition). The premixture with initial temperature T_0 and pressure P_0 is ignited from the center line in a 1D cylindrical chamber whose inner radius is R_W. Since, the end-gas is progressively compressed by the propagating flame, its temperature T_u and pressure P continuously increase. Similar to [17], the following assumptions were adopted in the present analysis: the 1D cylindrical flame is thin and smooth; the pressure is spatially uniform and changes only with time, i.e., $P = P(t)$; the burned and unburned gases behave as ideal gases; the unburned gas is compressed isentropically; and heat loss and buoyancy effects are negligible. Moreover,

Please cite this article as: H. Yu et al., Effects of flame propagation speed and chamber size on end-gas autoignition, Proceedings of the Combustion Institute (2016), http://dx.doi.org/10.1016/j.proci.2016.07.123

the following assumption of a linear relationship between BMF, x, and relative pressure rise [18] was adopted

$$x = 1 - m_u/m_0 = (P - P_0)/(P_e - P_0) \quad (1)$$

where the subscripts 0 and u, respectively, denote the initial states and states of unburned gas. The variables m, P, T and ρ denote mass per unit length, pressure, temperature and density, respectively. P_e is the equilibrium pressure (i.e., the pressure when the flame radius is $R_f = R_W$). Detailed numerical simulation in [19,32] demonstrated that the above linear relationship works well for 1D spherical flame propagating in a closed chamber. Similar demonstration was shown in Fig. S3 in the Supplementary material for 1D cylindrical flame.

When the flame radius is R_f, the mass of unburned gas per unit length is $m_u = \pi(R_W^2 - R_f^2)\rho_u$. The total mass, $m_0 = \pi R_W^2 \rho_0$, remains constant. Substituting these two equations into Eq. (1) yields [32]

$$R_f/R_W = \left[1 - (P_e - P)/(P_e - P_0)(P_0/P)^{1/\gamma_u}\right]^{1/2} \quad (2)$$

in which the isentropic relationship for unburned gas, $\rho_0/\rho_u = (P_0/P)^{1/\gamma_u}$, is used. Using Eq. (2) we can evaluate pressure P when the flame radius R_f is known or vice versa. At the moment of end-gas autoignition, the flame radius is denoted as R_i and the unburned gas has the pressure of P_i and temperature of $T_{u,i}$. Once R_i is given, we can solve Eq. (2) by setting $R_f = R_i$ and $P = P_i$ to get the pressure P_i, and then get the temperature $T_{u,i}$ from the isentropic relationship $T_{u,i}/T_0 = (P_i/P_0)^{(1-1/\gamma_u)}$. Under the assumptions that: (1) chemical reaction and heat release in end-gas are negligible before autoignition happens; and (2) the autoignition process occurs instantaneously at constant volume, we can obtain the maximum pressure, P_{max}, from equilibrium calculation based on the initial states of (P_i, $T_{u,i}$) at the moment of autoignition. Since chemical reaction does occur before autoignition, this assumption provides the most conservative estimate of P_{max} (i.e., the maximum pressure from the above equilibrium calculation is the upper limit). The maximum pressure from the above theoretical analysis will be compared with the counterpart from numerical simulations in Section 4. Equations (1) and (2) indicate that P increases with R_f. Therefore, if autoignition occurs at larger R_i, the BMF and the maximum pressure, P_{max}, both become higher, which indicates that P_{max} should increase monotonically with BMF.

According to the definition of laminar flame speed S_u, we have

$$dm_u/dt = -2\pi R_f \rho_u S_u. \quad (3)$$

Substituting Eqs. (1) and (2) into (3) yields

$$dt = R_W f(P) dP \text{ with } f(P) = \frac{\left[1 - (P_e - P)/(P_e - P_0)(P_0/P)^{1/\gamma_u}\right]^{-1/2}}{2(P_e - P_0)(P/P_0)^{1/\gamma_u} S_u}. \quad (4)$$

It is noted that laminar flame speed of unburned mixture, S_u, is a function of temperature T_u and pressure P. Since the unburned gas is compressed isentropically, T_u is a function of P and thus we have $S_u = S_u(T_u, P) = S_u(P)$. Similarly, for the ignition delay time of unburned mixture, we have $\tau_{ig} = \tau_{ig}(T_u, P) = \tau_{ig}(P)$.

Substituting Eq. (4) into the Livengood–Wu integral [6] yields

$$I = \int_0^t \frac{dt}{\tau_{ig}(T_u, P)} = R_W \int_{P_0}^{P} \frac{f(P)}{\tau_{ig}(P)} dP \text{ with } f(P) = \frac{\left[1 - (P_e - P)/(P_e - P_0)(P_0/P)^{1/\gamma_u}\right]^{-1/2}}{2(P_e - P_0)(P/P_0)^{1/\gamma_u} S_u(P)}. \quad (5)$$

End-gas autoignition occurs if the Livengood–Wu integral reaches unity before the flame front reaches the wall, i.e., $I = 1$ for $R_f < R_W$ or equivalently $P < P_e$ [6]. Equation (5) indicates that the Livengood–Wu integral is inversely proportional to S_u and proportional to R_W. Therefore, end-gas autoignition can be prevented by increasing flame propagation speed (i.e., larger S_u) or reducing chamber size (i.e., smaller R_W). When proper models or databases are used for the laminar flame speed $S_u = S_u(T_u, P)$ and ignition delay time $\tau_{ig} = \tau_{ig}(T_u, P)$, we can determine whether autoignition occurs based on the Livengood–Wu integral in Eq. (5). It in fact works reasonably well for hydrogen/air mixture as shown by Fig. S4 in the Supplementary material.

3. Numerical model, methods and specifications

As in theoretical analysis, in simulation we considered that 1D cylindrical flame propagates outwardly from the center of a closed chamber. The numerical model is the same as the one in our previous study [12] except that 1D cylindrical geometry instead of planar geometry was considered here. The propagating cylindrical flame was initialized by a hot kernel at the center whose radius is around 1 mm. Outside of the hot kernel is stoichiometric fuel/air mixture at the initial temperature of T_0. Two fuels were considered: hydrogen (due to its simple chemistry) and iso-octane (since it is the main component of the primary reference fuel, PRF, for gasoline). Initially the flow speed is zero (i.e., $u = 0$) everywhere and the initial pressure of P_0 is uniformly distributed in the computational

Please cite this article as: H. Yu et al., Effects of flame propagation speed and chamber size on end-gas autoignition, Proceedings of the Combustion Institute (2016), http://dx.doi.org/10.1016/j.proci.2016.07.123

domain $0 \le r \le R_W$. At both boundaries (i.e., $r = 0$ and $r = R_W$), zero flow speed and zero gradients of temperature and mass fractions were enforced. Although turbulence is important in engine combustion, here we focused on 1D laminar case in order to elucidate the mechanism for end-gas autoignition.

As in [12], the transient flame propagation and autoignition process were simulated using the in-house code A-SURF [20–23]. In A-SURF, the conservation equations for 1D compressible reactive flow were solved by finite volume method. A-SURF was successfully used in our studies on spherical flame propagation, end-gas autoignition and detonation development (e.g., [12,20,22,23,30,31]). The details on governing equations, numerical methods, and code validation for A-SURF can be found in Refs. [20–23] and were provided in the Supplementary material. For hydrogen and iso-octane, we used the detailed chemistry [24] and the skeletal mechanism [25], respectively. The skeletal mechanism was shown [25] to accurately predict the ignition delay and flame speed of PRF. To accurately resolve the propagation of flame front, adaptive mesh was used. The finest mesh size and time step size were 0.8 μm and 0.1 ns, respectively. Numerical convergence was checked and ensured by further decreasing the time step and mesh size in simulation.

To examine the effects of the flame propagation speed on end-gas autoignition, in simulation we introduced the artificial mass diffusivity, D_{artif}. For each species, its effective mass diffusivity is $D_{k,effect} = D_{artif} + D_k$, where D_k is the normal mass diffusivity of species k predicted by the mixture-averaged model. The effective thermal conductivity and viscosity were also obtained by adding artificial thermal conductivity and viscosity, respectively. The artificial thermal conductivity and artificial viscosity are both equal to the artificial mass diffusivity. Since the flame propagation speed increases monotonically with artificial mass diffusivity, D_{artif}, and the ignition delay time remains unchanged, we can assess the effects of flame propagation speed on end-gas autoignition by changing the magnitude of D_{artif}. To examine the effects of the chamber size on end-gas autoignition, in simulation we considered different chamber sizes, R_W.

4. Results and discussion

4.1. Hydrogen/air mixture

As mentioned in Section 2, Eq. (5) from theoretical analysis indicates that end-gas autoignition can be prevented by increasing flame propagation speed (i.e., larger S_u or larger D_{artif}) or reducing chamber size (i.e., smaller R_W). This was demonstrated by the results in Fig. 1, which plots the normalized flame radius for different values of artificial mass diffusivity and chamber size. The onset of autoignition was determined based on heat release rate and pressure from 1D simulations rather than the Livengood–Wu integral. For the reference case with $R_W = 2$ cm and $D_{artif} = 0$ m^2/s (line #3 in Fig. 1), end-gas autoignition occurs at $t = 425$ μs and $R_f = 0.95$ cm. When D_{artif} is increased from zero to 5×10^{-4} m^2/s (line #2), the flame propagation speed (proportional to the slope in Fig. 1) increases and thereby there is no end-gas autoignition. When the chamber size is reduced to $R_W = 0.8$ cm (line #1), end-gas autoignition also disappears. On the contrary, a larger chamber size of $R_W = 4$ cm (line #4) facilitates end-gas autoignition.

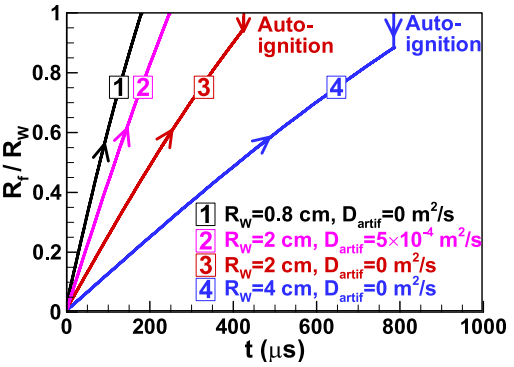

Fig. 1. Change of normalized flame front position, R_f / R_W, with time for stoichiometric H_2/air mixture with $T_0 = 975$ K and $P_0 = 10$ atm.

Figure 2 shows the near-wall pressure history at different values of D_{artif} and R_W for stoichiometric H_2/air at $T_0 = 975$ K and $P_0 = 10$ atm (= 10.13 bar). End-gas autoignition occurs for cases corresponding to lines #1–5 in both Fig. 2(a) and (b). At the beginning, the pressure rises gradually. When end-gas autoignition occurs, there is a sudden pressure rise due to the global thermal explosion in end-gas. After the sharp pressure rise, pressure oscillation appears since the pressure wave propagates back-and-forth in the closed chamber. The maximum pressure, P_{max}, for autoignition cases is much higher than the equilibrium value of $P_e = 28.0$ atm. Consistent with Eq. (5) from theoretical analysis, Fig. 2 shows that when S_u (equivalently D_{artif}) is large enough or R_W is small enough (line #6), end-gas autoignition can be prevented and P_{max} is close to the equilibrium value of $P_e = 28.0$ atm. This fact is also shown by Fig. 3 in which the open symbols denote cases without end-gas autoignition.

Figure 3 shows that the normalized flame radius at the time of end-gas autoignition, R_i/R_W, increases monotonically with D_{artif} and it decreases monotonically with R_W. This is consistent with theoretical analysis that end-gas autoigni-

Please cite this article as: H. Yu et al., Effects of flame propagation speed and chamber size on end-gas autoignition, Proceedings of the Combustion Institute (2016), http://dx.doi.org/10.1016/j.proci.2016.07.123

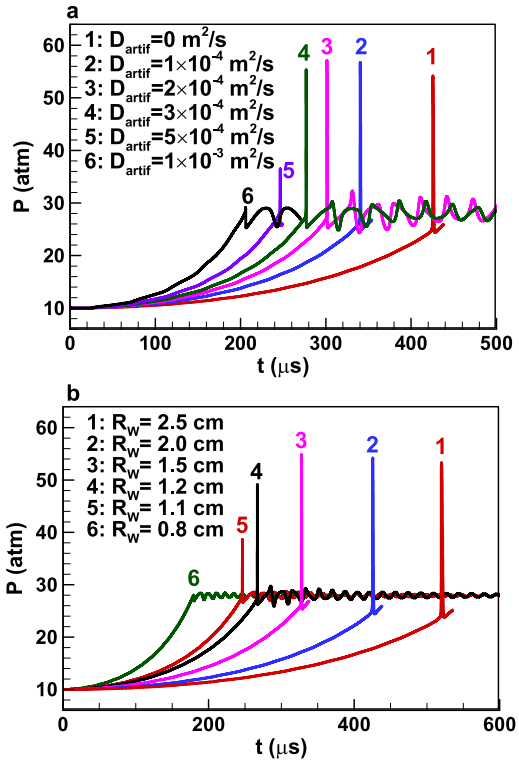

Fig. 2. Temporal evolution of pressure near the wall: (a) different artificial diffusivities with fixed $R_W = 2.0$ cm; (b) different chamber sizes with fixed $Dartif = 0\ m^2/s$. The mixture is stoichiometric H_2/air at $T_0 = 975$ K and $P_0 = 10$ atm.

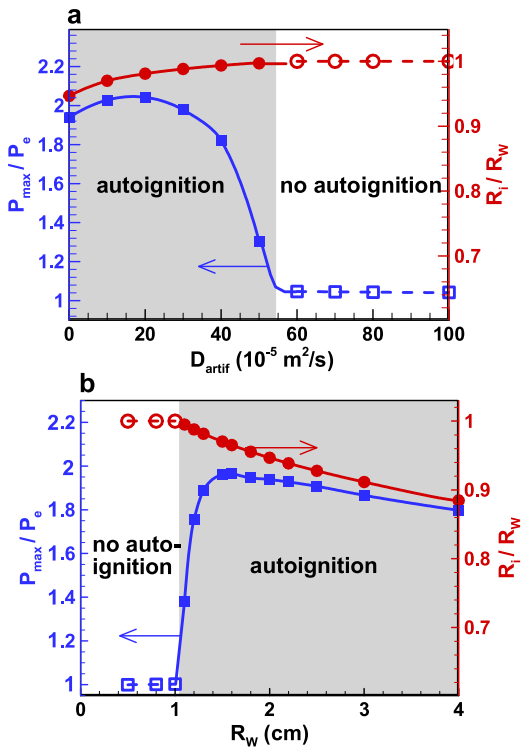

Fig. 3. Influence of (a) artificial diffusivity and (b) chamber size on the normalized autoignition flame radius, R_i/R_W, and maximum pressure, P_{max}/P_e. The mixture is stoichiometric H_2/air at $T_0 = 975$ K and $P_0 = 10$ atm.

tion can be prevented by increasing the flame propagation speed (i.e., increasing D_{artif}) or decreasing the chamber size R_W. However, Fig. 3 also shows that the normalized maximum pressure, P_{max}/P_e, changes non-monotonically with D_{artif} and R_W: it first increases and then decreases with the increase (decrease) of D_{artif} (R_W). Therefore, the maximum pressure does not change monotonically with flame propagation speed or chamber size. Such non-monotonic change causes the contradiction on whether faster combustion may promote or inhibit end-gas autoignition and engine knock. Figure 3(a) indicates that if the flame propagation is fast enough (i.e., D_{artif} is large enough), end-gas autoignition and knock can be prevented; otherwise, the knock intensity may increase with the flame propagation speed.

To explain the non-monotonic change of P_{max} with D_{artif} and R_W, in Fig. 4 we plotted different normalized pressures as a function of normalized autoignition flame radius, R_i/R_W. The corresponding BMF, x, at the time of end-gas autoignition is also depicted in Fig. 4. It is observed that the theoretical results, $P_{i,\,theory}$ and $P_{max,\,theory}$, both increase monotonically with R_i/R_W. This is

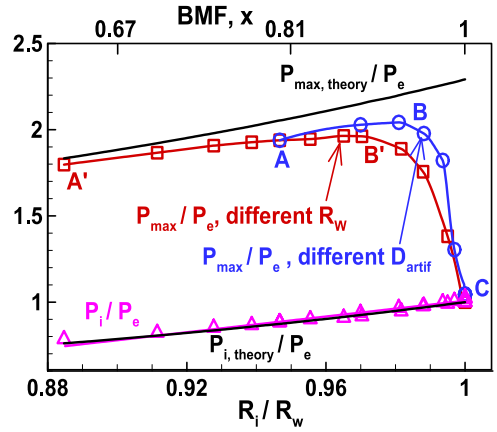

Fig. 4. Normalized pressures as a function of normalized autoignition flame radius. The corresponding burned mass fraction (BMF) is also displayed. The symbols denote simulation results and black lines represent theoretical results. The mixture is stoichiometric H_2/air at $T_0 = 975$ K and $P_0 = 10$ atm.

Please cite this article as: H. Yu et al., Effects of flame propagation speed and chamber size on end-gas autoignition, Proceedings of the Combustion Institute (2016), http://dx.doi.org/10.1016/j.proci.2016.07.123

because when autoignition occurs at larger R_i/R_W, the end-gas is compressed to higher pressure (i.e., the pressure right before autoignition, $P_{i,\,theory}$, is higher) according to Eq. (2), and thus the maximum pressure after autoignition, $P_{max,\,theory}$, also becomes higher. Since end-gas is not chemically frozen and there are weak chemical reactions and heat release before autoignition occurs, the numerical results, P_{max}, are smaller than the theoretical results, $P_{max,\,theory}$. For numerical results in Fig. 4, D_{artif} increases along the curve ABC and R_W decreases along the curve A′B′C. End-gas autoignition does not occur at point C when D_{artif} is large enough or R_W is small enough. When R_i/R_W is not very close to unity (e.g., $R_i/R_W < 0.97$), the trend along AB and A′B′ is shown to be the same as that predicted by theory: P_{max} from simulation increases with R_i/R_W or BMF. This indicates that the knock intensity increases as the flame propagation speed increases or the chamber size decreases and that the knock intensity increases with BMF. When R_i/R_W is close to unity (e.g., $0.98 < R_i/R_W < 1$), the trend along BC and B′C is opposite to that predicted by theory: P_{max} from simulation decreases with R_i/R_W or BMF. This indicates that the knock intensity decreases as the flame propagation speed increases or the chamber size decreases and that the knock intensity decreases with BMF. This is due to the facts that when R_i/R_W is close to unity, there is only a small amount of unburned mixture in the end-gas which cannot support nearly constant-volume autoignition (the heat release at the moment of autoignition is not infinite fast and thereby the pressure rise due to heat release is damped by pressure wave propagating at sound speed); and that the theoretical results for $P_{max,\,theory}$ were obtained based on the assumption of constant-volume autoignition of end-gas. The non-monotonic change of P_{max} with BMF helps to clarify the contradiction on whether knock intensity increases or decreases with BMF.

To check whether constant-volume autoignition always occurs in end-gas, we tracked the thermal states of the fluid particle near the wall boundary [12]. The results are plotted in Fig. 5. For $R_W = 2.5$ cm, end-gas autoignition happens and the near-wall particle goes through three stages: isentropic compression along OA; nearly constant-volume autoignition along AF; and expansion FH. It is the nearly constant-volume autoignition that causes the rapid pressure rise observed in Fig. 2(b). When the chamber size is reduced to $R_W = 1.5$ cm, end-gas autoignition occurs at relatively smaller specific volume and higher pressure at point B and consequently the maximum pressure at point E is higher than that at point F for $R_W = 2.5$ cm. This is consistent with the fact that maximum pressure increases as the chamber size decreases (i.e., P_{max} increases with R_i/R_W along A′B′ in Fig. 4). However, when the chamber size is further reduced to $R_W = 1.1$ cm (line OCGH in Fig. 5), end-gas

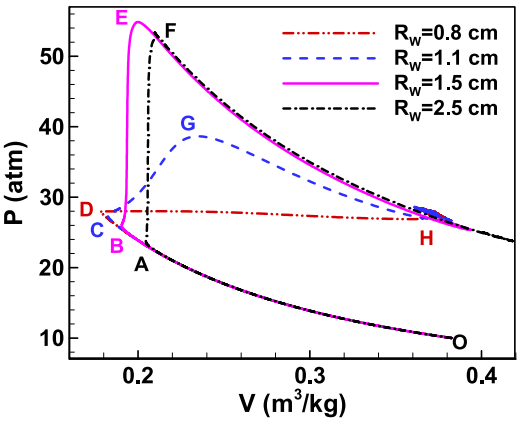

Fig. 5. The pressure versus specific volume, P–V, diagram for particle near the wall boundary. Different chamber sizes, $R_W = 0.8$–2.5 cm, with fixed $D_{artif} = 0\ m^2/s$. The mixture is stoichiometric H_2/air at $T_0 = 975$ K and $P_0 = 10$ atm.

autoignition occurs at $R_i/R_W = 0.995$ and the autoignition process along CG is no longer constant-volume: the specific volume increases along CG due to expansion. Consequently, the maximum pressure at point G is much lower than those at points E and F. This is consistent with the fact that maximum pressure decreases as the chamber size decreases (i.e., P_{max} decreases with R_i/R_W along B′C in Fig. 4). When the chamber size is small enough, e.g., $R_W = 0.8$ cm, there is no end-gas autoignition and Fig. 5 indicates that the particle goes through nearly constant-pressure combustion along DH; consequently, the maximum pressure is close to the equilibrium value of $P_e = 28.0$ atm.

The above results are only for stoichiometric H_2/air mixture at $T_0 = 975$ K and $P_0 = 10$ atm. Figure 6 shows the results at different values of T_0, P_0, D_{artif} and R_W. Similar to Fig. 4, Fig. 6 shows that there are two regimes. In regime I with $R_i/R_W < 0.974$, P_{max} increases with R_i/R_W and thereby the maximum pressure increases as the flame propagation speed increases or the chamber size decreases; while in regime II with $0.974 < R_i/R_W < 1$, the opposite trend occurs. In regimes I and II, the maximum pressure, respectively, increases and decreases with BMF.

In a short summary, the results above help to explain why there is contradictory literature on (1) whether faster combustion may promote or inhibit end-gas autoignition and engine knock, and (2) whether knock intensity increases or decreases with BMF. The answers to these two questions depend on the amount of unburned mixture at the moment of end-gas autoignition: if there is enough unburned mixture before end-gas autoignition, the maximum pressure increases with the flame

Please cite this article as: H. Yu et al., Effects of flame propagation speed and chamber size on end-gas autoignition, Proceedings of the Combustion Institute (2016), http://dx.doi.org/10.1016/j.proci.2016.07.123

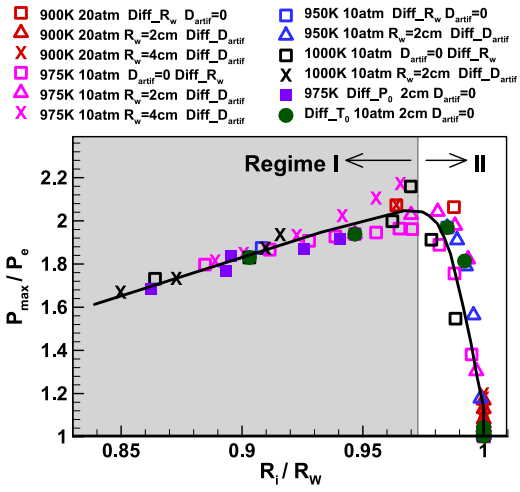

Fig. 6. Normalized maximum pressure as a function of normalized autoignition flame radius for stoichiometric H_2/air mixture at different values of T_0, P_0, D_{artif} and R_W.

propagation speed and BMF; otherwise, the opposite trend occurs.

4.2. Iso-octane/air mixture

To demonstrate that the above conclusions are fuel-independent, we considered another fuel, iso-octane. Similar results were obtained and only those for stoichiometric iC_8H_{18}/air at $T_0 = 650$ K and $P_0 = 20$ atm are shown here due to space limit.

Figure 7 shows the influence of artificial diffusivity (or flame propagation speed) and chamber size on the autoignition position and maximum pressure for iC_8H_{18}/air. It is seen that R_i/R_W increases (decreases) monotonically with D_{artif} (R_W); and that P_{max}/P_e changes non-monotonically with D_{artif} and R_W. Such trends are the same as those for H_2/air in Fig. 3.

Figure 8 shows different normalized pressures as a function of normalized autoignition flame radius for iC_8H_{18}/air. Again, these results are similar to those for H_2/air in Fig. 4. Due to the chemical reaction and heat release occurring before autoignition, the numerical results, P_i and P_{max}, are respectively larger and smaller than the theoretical results, $P_{i,\,theory}$ and $P_{max,\,theory}$. The main difference is that $P_{max,\,theory}$-P_{max} for iC_8H_{18}/air is much larger than that for H_2/air (compare Fig. 8b and Fig. 4). This is mainly due to the fact that before end-gas autoignition, more low-temperature reaction and heat release happen in iC_8H_{18}/air than in H_2/air, which are demonstrated by results in Figs. 9 and 10. Similar explanation works for the well-known fact that fuels with two-stage ignition are better-suited for HCCI because peak pressures are reduced.

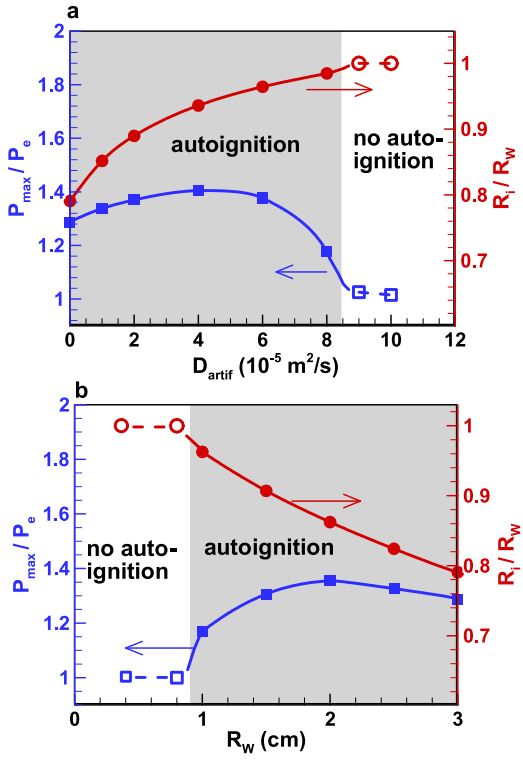

Fig. 7. Influence of (a) artificial diffusivity and (b) chamber size on the normalized autoignition position, R_i/R_W, and maximum pressure, P_{max}/P_e. The mixture is stoichiometric iC_8H_{18}/air mixture at $T_0 = 650$ K and $P_0 = 20$ atm.

Figure 9 shows the P–V diagrams for particles near the wall boundary; and Fig. 10 depicts the evolution of the pressure and heat release rate for the near-wall particle in the chamber of $R_W = 2$ cm. In Fig. 10, points B′, G′ and H′ denote three peaks of heat release rate (the corresponding temperature is 810, 1290 and 2900 K, respectively). Therefore, the turning points, A, B, C and D in Fig. 9 are caused by low-temperature heat release. For $R_W = 0.8$ cm, there is no end-gas autoignition and the main heat release occurs along curve EF under nearly constant-pressure condition. For the case with end-gas autoignition, e.g., $R_W = 2.0$ cm, the process is much more complicated: first the particle goes through isentropic compression along OB; then low-temperature heat release occurs around point B, after which it is further compressed along BJ; then the intermediate-temperature heat release occurs with the peak at point G; and finally heat is released by high-temperature reactions and the pressure sharply increases along KH. Comparison between Figs. 5 and 9 indicates that there is much more heat release in iC_8H_{18}/air than in H_2/air before end-gas autoigni-

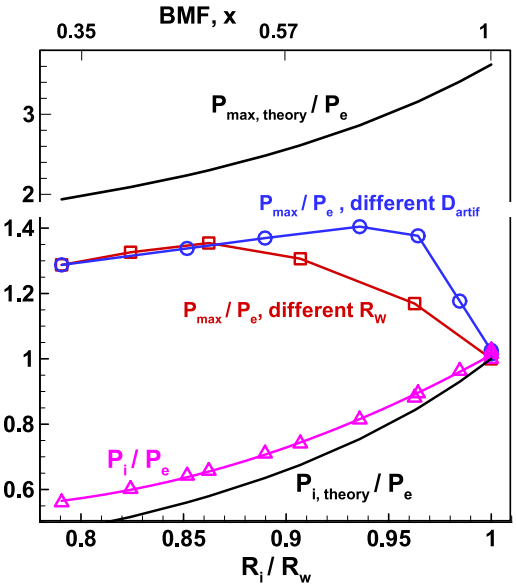

Fig. 8. Normalized pressures as a function of normalized autoignition flame radius. The corresponding burned mass fraction (BMF) is also displayed. The symbols denote simulation results and black lines represent theoretical results. The mixture is stoichiometric iC_8H_{18}/air mixture at $T_0 = 650$ K and $P_0 = 20$ atm.

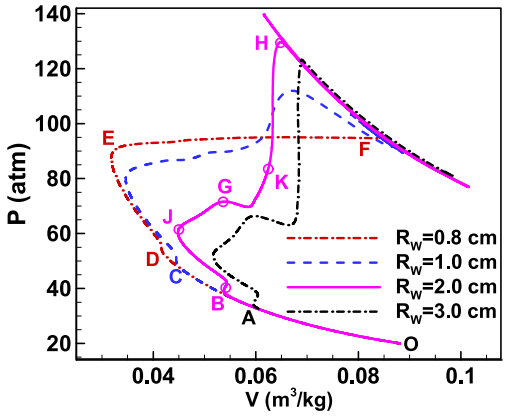

Fig. 9. The pressure versus specific volume, P–V, diagram for particle near the wall boundary. Different chamber sizes, $R_W = 0.8$–3.0 cm, with fixed $D_{artif} = 0$ m^2/s. The mixture is stoichiometric iC_8H_{18}/air mixture at $T_0 = 650$ K and $P_0 = 20$ atm.

tion occurs. This explains why $P_{max,\,theory}$-P_{max}, for iC_8H_{18}/air is much larger than that for H_2/air.

5. Conclusions

In this work, the influence of flame propagation speed and chamber size on end-gas autoignition and maximum pressure is examined by theoretical analysis and simulation of 1D propagating cylindrical flame in a closed chamber. An artificial diffusivity, D_{artif}, is used in simulation to modify the flame propagation speed. It is demonstrated that if the flame propagation is fast enough or the chamber is small enough, end-gas autoignition and knock can be prevented; otherwise, the maximum pressure may increase as the flame propagation speed increases or the chamber size decreases. Two regimes are identified in the plot of normalized maximum pressure versus normalized autoignition flame radius (see Figs. 6, 4 and 8): in regime I with relative small BMF, the maximum pressure increases as the flame propagation speed increases or the chamber size decreases; while in regime II with BMF close to unity, the opposite trend occurs. The opposite change of maximum pressure with flame propagation speed in regimes I and II helps to explain the contradictory literature about the influence of flame speed on end-gas autoignition and engine knock. In regimes I and II, the maximum pressure, respectively, increases and decreases with BMF, which helps to clarify the contradiction on whether knock intensity increases or decreases with BMF. Besides, the simulation results for i-C_8H_{18}/air mixture indicate that chemical reaction and heat release in end-gas before autoignition can greatly reduce the maximum pressure.

It is noted that in the present study the chamber volume remains constant. This is unlike the real engine in which the chamber volume is time-dependent. The compression and expansion due to chamber volume change are expected to affect end-gas autoignition and it deserves further study.

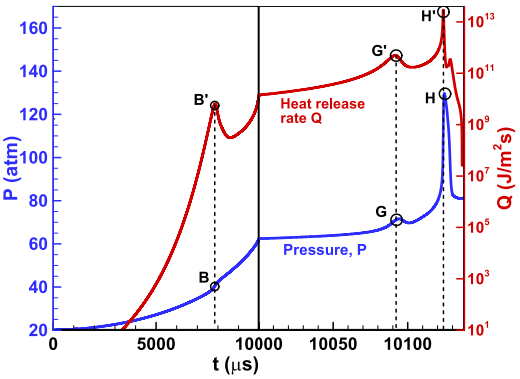

Fig. 10. Evolution of pressure and heat release rate for particle near the wall boundary for $R_W = 2$ cm shown in Fig. 9.

Acknowledgment

This work was supported by National Natural Science Foundation of China (No. 51322602)

Please cite this article as: H. Yu et al., Effects of flame propagation speed and chamber size on end-gas autoignition, Proceedings of the Combustion Institute (2016), http://dx.doi.org/10.1016/j.proci.2016.07.123

and State Key Laboratory of Engines at Tianjin University (No. K2014-01). We acknowledge helpful discussions with Prof. Yiguang Ju at Princeton University and Profs. Xin He and Zhi Wang at Tsinghua University.

Supplementary materials

Supplementary material associated with this article can be found, in the online version, at doi:10.1016/j.proci.2016.07.123.

References

[1] J.B. Heywood, *Internal Combustion Engine Fundamentals*, McGraw Hill, New York, 1988.
[2] J. Pan, G. Shu, H. Wei, *Combust. Sci. Technol.* 186 (2014) 192–209.
[3] D. Bradley, *J. Chem. Soc. Faraday* 92 (1996) 2959–2964.
[4] L.S. Kagan, P.V. Gordon, G.I. Sivashinsky, *Combust. Theory Model.* 16 (2012) 1–12.
[5] L. Kagan, G. Sivashinsky, *Proc. Combust. Inst.* 34 (2013) 857–863.
[6] J.C. Livengood, P.C. Wu, *Proc. Combust. Inst.* 5 (1955) 347–356.
[7] M. Pöschl, T. Sattelmayer, *Combust. Flame* 153 (2008) 562–573.
[8] N. Kawahara, E. Tomita, Y. Sakata, *Proc. Combust. Inst.* 31 (2007) 2999–3006.
[9] J. Pan, C.G.W. Sheppard, *SAE 942060* (1994).
[10] M.A. Liberman, M.F. Ivanov, D.M. Valiev, L.E. Eriksson, *Combust. Sci. Technol.* 178 (2006) 1613–1647.
[11] H. Terashima, M. Koshi, *Combust. Flame* 162 (2015) 1944–1956.
[12] H. Yu, Z. Chen, *Combust. Flame* 162 (2015) 4102–4111.
[13] Y. Chen, R. Raine, *Combust. Flame* 162 (2015) 2108–2118.
[14] H. Hirooka, S. Mori, R. Shimizu, SAE 2004-01-0977.
[15] Y. Chen, R. Raine, *SAE Int. J. Engines* 7 (2014) 595–605.
[16] A. Robert, S. Richard, O. Colin, T. Poinsot, *Combust. Flame* 162 (2015) 2788–2807.
[17] D. Bradley, A. Mitcheson, *Combust. Flame* 26 (1976) 201–217.
[18] B. Lewis, G. Von Elbe, *Combustion, Flames and Explosions of Gases*, Elsevier, 2012.
[19] Z. Chen, M.P. Burke, Y. Ju, *Combust. Theory Model.* 13 (2009) 343–364.
[20] Z. Chen, M.P. Burke, Y. Ju, *Proc. Combust. Inst.* 32 (2009) 1253–1260.
[21] Z. Chen, *Combust. Flame* 157 (2010) 2267–2276.
[22] P. Dai, Z. Chen, S. Chen, Y. Ju, *Proc. Combust. Inst.* 35 (2015) 3045–3052.
[23] P. Dai, Z. Chen, *Combust. Flame* 162 (2015) 4183–4193.
[24] J. Li, Z. Zhao, A. Kazakov, F.L. Dryer, *Int. J. Chem. Kinet.* 36 (2004) 566–575.
[25] H. Wang, M. Yao, R.D. Reitz, *Energy Fuel* 27 (2013) 7843–7853.
[26] A. Bhagatwala, J.H. Chen, T. Lu, *Combust. Flame* 161 (2014) 1826–1841.
[27] A. Bhagatwala, R. Sankaran, S. Kokjohn, J.H. Chen, *Combust. Flame* 162 (2015) 3412–3426.
[28] M.B. Luong, Z. Luo, T. Lu, S.H. Chung, C.S. Yoo, *Combust. Flame* 160 (2013) 2038–2047.
[29] S.O. Kim, M.B. Luong, J.H. Chen, C.S. Yoo, *Combust. Flame* 162 (2015) 717–726.
[30] Z. Chen, *Combust. Flame* 162 (2015) 2242–2253.
[31] H. Yu, W. Han, J. Santner, et al., *Combust. Flame* 161 (2014) 2815–2824.
[32] M. Faghih, Z. Chen, *Sci. Bull.* 61 (2016) 1296–1310.

Please cite this article as: H. Yu et al., Effects of flame propagation speed and chamber size on end-gas autoignition, Proceedings of the Combustion Institute (2016), http://dx.doi.org/10.1016/j.proci.2016.07.123